

## Short Communication

# Suitable acidity of ZSM-5 for the isomerization of styrene oxide to phenylacetaldehyde



Ming-Lei Gou, Rijie Wang, Qiwei Qiao, Xiaoxia Yang\*

School of Chemical Engineering and Technology, Tianjin University, Tianjin 300072, PR China

## ARTICLE INFO

## Article history:

Received 17 March 2014

Received in revised form 16 June 2014

Accepted 15 July 2014

Available online 24 July 2014

## Keywords:

ZSM-5

Acidity

Isomerization

Styrene oxide

Phenylacetaldehyde

## ABSTRACT

The effect of acidity of HZSM-5 ( $\text{SiO}_2/\text{Al}_2\text{O}_3 = 25\text{--}360$ ) on isomerization of styrene oxide to phenylacetaldehyde was investigated under gas-phase free of solvents. The reaction was mainly catalyzed by the strong acid sites of HZSM-5 and catalyst lifetimes were affected by both acid strength and concentration. Trimerization of phenylacetaldehyde occurred at external acid sites, leading to a sharp decline in product selectivity. High Si/Al HZSM-5 (e.g.,  $\text{SiO}_2/\text{Al}_2\text{O}_3 = 360$ ), which contains weaker acid sites inside pores and trace amount of external acid sites, was found to be more effective with a higher stability and phenylacetaldehyde yield up to 95%.

© 2014 Elsevier B.V. All rights reserved.

## 1. Introduction

Phenylacetaldehyde, giving a narcissus-like smell, is an important fine chemical used for preparation of fragrances, pharmaceuticals, insecticides, fungicides and herbicides [1]. Hoelderich et al. [2,3] have previously reported that phenylacetaldehyde and its halogenated derivatives can be obtained via isomerization of styrene oxide and its halogenated styrene oxides over acid catalysts. However, the competitive aldol condensation or polymerization of aldehyde products and fast deactivation of catalysts by coke formation are still difficult problems at the industrial scale [1].

A series of heterogeneous catalysts, such as alkaline earth metal sulfonates [4], mixed-metal oxides [5], silica–alumina gels [6,7], natural silicates [8], Nafion-H [9], zeolites [10–12] and heteropoly acids [13], have all been applied as catalysts for the isomerization of epoxides to aldehydes. It can be seen that the active sites from weakly alkaline to strong acidic can catalyze this reaction, but the aldol condensation or polymerization can readily occur on alkaline [4,5] and strong acid sites [13–15], resulting in rapid deactivation of catalysts. Consequently, there is a need to find a suitable acid catalyst, which not only has high activity and stability, but also prohibits side reactions. However, detailed investigation on this topic has not yet been published.

It is reported that zeolites of the mordenite, erionite and chabazite types are all suitable to catalyze this reaction, particularly, zeolites of the MFI type have the best performance with phenylacetaldehyde yield up to 90% at 200 °C and  $\text{WHSV} = 3 \text{ h}^{-1}$ , but the catalysts

deactivate within 6 h on stream [3]. The acidity of zeolites usually depends on the nature and amount of the framework aluminum atoms [16,17]. Therefore, a series of ZSM-5 zeolites with  $\text{SiO}_2/\text{Al}_2\text{O}_3$  ratios of 25–360 were chosen as catalysts to determine the effect of acidity on the reaction. Catalysts were characterized by XRF, nitrogen adsorption, XRD,  $\text{NH}_3$ -TPD/titration, FT-IR spectra of pyridine and 2,4,6-trimethyl pyridine adsorption.

## 2. Experimental

## 2.1. Materials

Styrene oxide (>98%) was purchased from TCI (Shanghai) Development Co., Ltd. and used without further purification. HZSM-5 ( $\text{SiO}_2/\text{Al}_2\text{O}_3 = 25\text{--}360$ ) and NaZSM-5 ( $\text{SiO}_2/\text{Al}_2\text{O}_3 = 25$ ) were all obtained from Catalyst Plant of Nankai University (Tianjin, PR China) and denoted as HZ-x and NaZ-x, where x referred to the  $\text{SiO}_2/\text{Al}_2\text{O}_3$  ratio according to manufacturer's specifications.

## 2.2. Catalyst characterization

The chemical composition of the catalysts was determined by X-ray fluorescence (XRF) with a Bruker S4 Pioneer X-ray fluorescence spectrometer. Nitrogen adsorption was performed using a Quantachrome Autosorb-1 instrument at 77 K, after a vacuum pretreatment at 250 °C for 6 h. The surface area was calculated according to the Brunauer–Emmett–Teller (BET) equation. The pore volume and size were estimated from the Horvath–Kawazoe (HK) method. Powder X-ray diffraction (XRD) patterns were recorded on a PANalytical X'Pert Pro diffractometer

\* Corresponding author. Tel./fax: +86 22 27401018.  
E-mail address: [xyx@tju.edu.cn](mailto:xyx@tju.edu.cn) (X. Yang).

equipped with a Co K $\alpha$  radiation ( $\lambda = 0.1789$  nm). Data were collected in the range of  $2\theta = 5\text{--}50^\circ$  with a step size of  $0.02^\circ$  at a scanning speed of  $5^\circ/\text{min}$ .

The acidic properties of the catalysts were studied by temperature-programmed desorption of ammonia ( $\text{NH}_3$ -TPD) and FT-IR spectra of adsorbed pyridine and 2,4,6-trimethylpyridine (collidine).  $\text{NH}_3$ -TPD was performed on a conventional apparatus equipped with a thermal conductivity detector. The sample (100 mg, 20–30 mesh) was pretreated at  $500^\circ\text{C}$  for 2 h with a  $\text{N}_2$  flow (50 ml/min) and then cooled down to ambient temperature. Sufficient  $\text{NH}_3$  was supplied to the system followed by flushing with  $\text{N}_2$  at  $150^\circ\text{C}$  for 1 h. The TPD profile was obtained by heating the sample from  $150$  to  $500^\circ\text{C}$  at a rate of  $15^\circ\text{C}/\text{min}$ . The  $\text{NH}_3$  desorbing between  $150$  and  $500^\circ\text{C}$  was trapped in boric acid and then titrated with a standard  $\text{H}_2\text{SO}_4$  solution [18]. According to the individual peak area, the amount of  $\text{NH}_3$  can be calculated and then converted into the acid concentrations with the assumption of one  $\text{NH}_3$  molecule per acid site.

FT-IR spectra of adsorbed pyridine and collidine were recorded on a Nicolet 380 spectrometer at  $4\text{ cm}^{-1}$  resolution. The sample powder was pressed into a self-supporting wafer (diameter: 13 mm, weight: 15 mg) and activated at  $500^\circ\text{C}$  for 2 h under vacuum ( $10^{-3}$  Pa). Probe molecule adsorption was taken place in situ at room temperature, followed by evacuation at  $200^\circ\text{C}$  for 1 h. Afterwards, an IR spectrum was recorded at room temperature and a difference spectrum was obtained by subtracting the spectrum of the activated sample from the spectrum after probe adsorption.

### 2.3. Isomerization of styrene oxide

Isomerization was carried out in a vertical fixed-bed reactor (stainless steel tube, i.d. = 9 mm) operated at atmospheric pressure. Prior to each experiment, the sample (0.5 g, 20–30 mesh) located in the constant-temperature zone was treated in a  $\text{N}_2$  flow at  $500^\circ\text{C}$  for 2 h. After cooling to reaction temperature ( $200^\circ\text{C}$ ), styrene oxide, free of any solvents, was fed with  $\text{WHSV} = 3.0\text{ h}^{-1}$  using a HPLC pump (model Series II, LabAlliance, USA).  $\text{N}_2$  was used as the carrier gas, with a flow-rate of 120 ml/min, during the reaction. The reactor effluent was collected in an ice trap and analyzed by GC (Agilent 6820 FID) and GC-MS (Agilent 6890/5973 MSD) equipped with VF-5ms capillary column (30 m, 0.25 mm, 0.25  $\mu\text{m}$ ).

## 3. Results and discussion

### 3.1. Characterization results

The chemical composition and some physical properties of the catalysts are listed in Table 1. The bulk  $\text{SiO}_2/\text{Al}_2\text{O}_3$  molar ratios determined by XRF were in good agreement with the values given by the manufacturer. All the samples showed typical type-I isotherms (figures not shown here), indicating uniform micropore structures according to IUPAC classification. The BET surface area, micropore volume and size were all similar to each other, suggesting that their textural properties did not lead to different catalytic performances.

**Table 1**  
Chemical composition and physical properties of the catalysts.

Sample	$\text{SiO}_2/\text{Al}_2\text{O}_3$ (mol/mol)	BET surface area ( $\text{m}^2/\text{g}$ )	Pore volume ( $\text{cm}^3/\text{g}$ )	Pore size ( $\text{\AA}$ )	Relative crystallinity (%)
NaZ-25	26.8	291.5	0.145	4.6	84
HZ-25	26.8	291.6	0.145	4.6	80
HZ-38	39.1	290.5	0.145	4.6	82
HZ-50	49.7	291.2	0.145	4.6	100
HZ-135	134.6	290.4	0.144	4.6	97
HZ-150	151.2	290.5	0.144	4.6	99
HZ-360	362.0	289.1	0.142	4.6	98

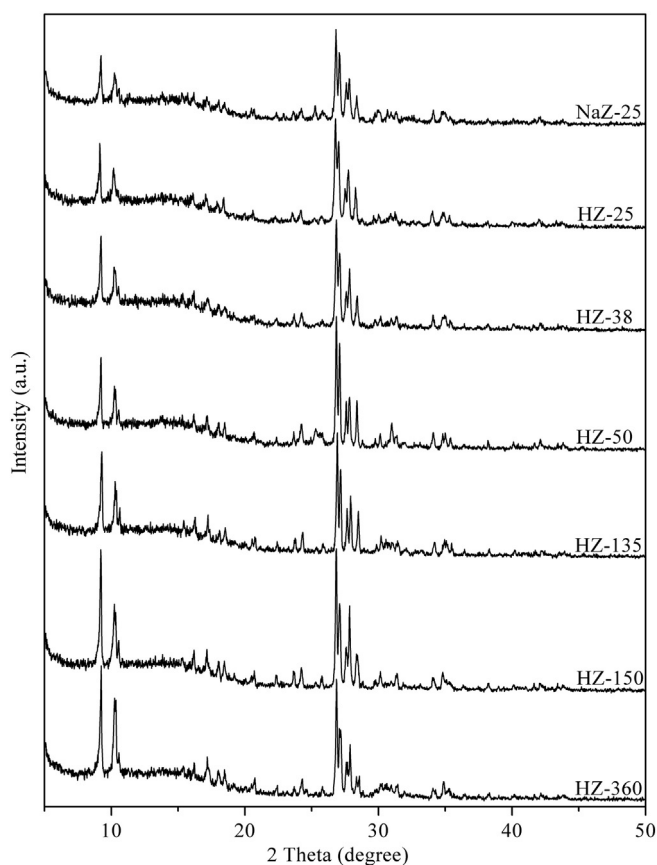


**Fig. 1.** XRD patterns of the catalysts.

The XRD patterns of the catalysts in Fig. 1 matched well with typical MFI-type structures and presented no additional phase. HZ-50 had the highest intensity and the relative crystallinity was obtained from the peaks' area of  $2\theta = 26\text{--}29^\circ$  using HZ-50 as a reference for this study. As shown in Table 1, HZ-25 and HZ-38 had slightly lower relative crystallinity than other samples. This is probably due to more amorphous Si or Al species formed in either micropores or alongside the channels of ZSM-5 catalysts with lower Si/Al ratios during the ion-exchange with  $\text{NH}_4^+$  and calcinations.

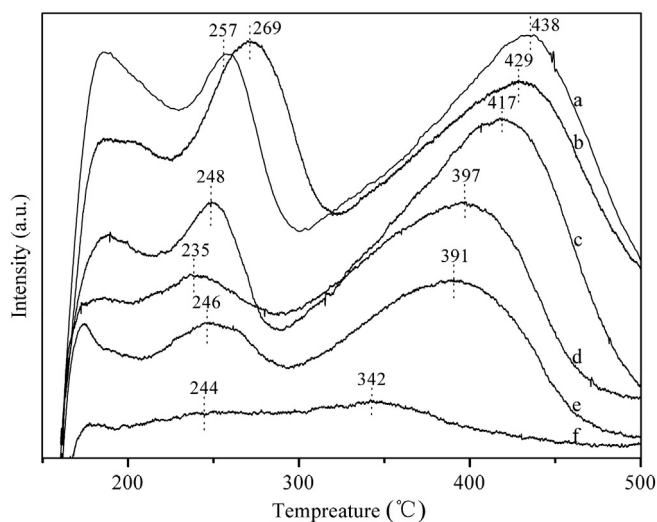


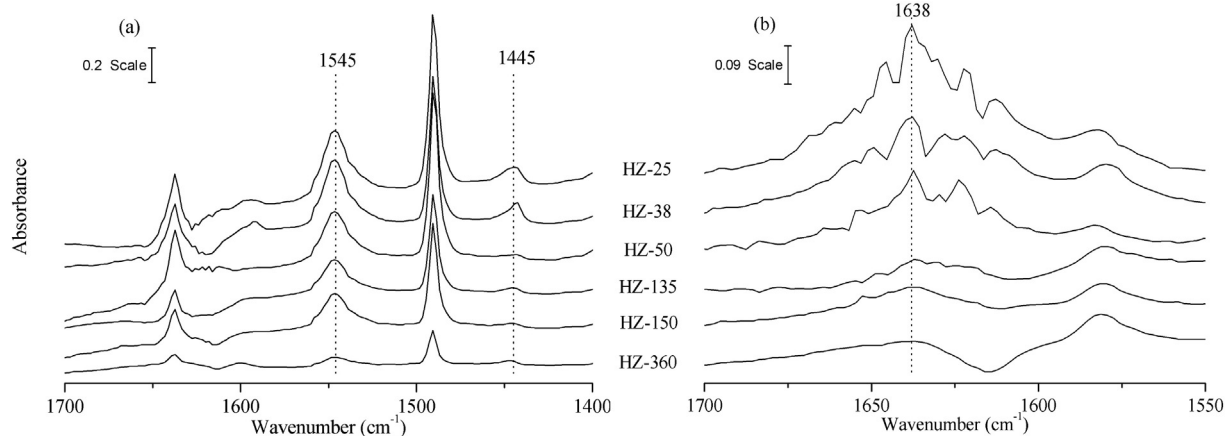
**Fig. 2.**  $\text{NH}_3$ -TPD profiles of the HZSM-5 zeolites. (a) HZ-25, (b) HZ-38, (c) HZ-50, (d) HZ-135, (e) HZ-150 and (f) HZ-360.

**Table 2**  
Acidic properties of the catalysts.

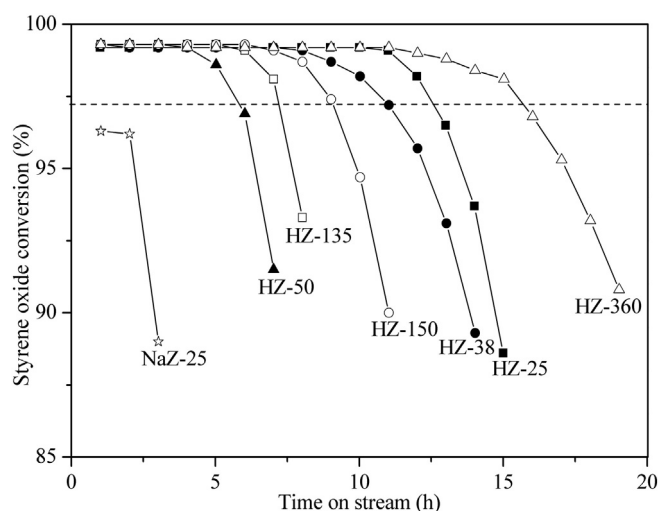
Sample	Weak acid sites (mmol/g)	Strong acid sites (mmol/g)	Brønsted/Lewis (mol/mol)	External acid sites (IA, cm <sup>-1</sup> )
NaZ-25	0.072	–	–	–
HZ-25	0.169	0.606	6.2	0.224
HZ-38	0.234	0.416	5.5	0.186
HZ-50	0.143	0.336	25.3	0.117
HZ-135	0.114	0.256	13.1	Trace
HZ-150	0.095	0.207	12.2	Trace
HZ-360	0.021	0.048	7.3	Trace

Fig. 2 illustrates the NH<sub>3</sub>-TPD profiles of the samples, and the acid concentrations of differing strengths are given in Table 2. All the HZSM-5 samples had three NH<sub>3</sub>-desorption peaks at <200, 239–269 and 342–438 °C. The one below 200 °C was attributed to the desorption of physisorbed ammonia, while the other two represented ammonia desorption from weak and strong acid sites [19,20]. The strong acid sites were typically known as Brønsted acid sites (Si–OH–Al). With increasing Si/Al ratio, the high-temperature peak gradually shifted to a lower temperature and lost its intensity, suggesting that the strength and concentration of strong acid sites decreased. The concentration of weak acid sites showed the same trend as the strong acid sites (Table 2), while the weak acid strengths differed little from each other. NaZ-25 produced only one NH<sub>3</sub>-desorption peak centered around 248 °C (not shown here), indicating that the sample had only some weak acid sites (0.072 mmol/l).

The difference FT-IR spectra of adsorbed pyridine and collidine on the HZSM-5 samples are shown in Fig. 3. In Fig. 3(a), the bands at 1545 cm<sup>-1</sup> and 1455 cm<sup>-1</sup> were attributed to pyridine bound to Brønsted and Lewis acid sites [21]. The intensity of the band at 1545 cm<sup>-1</sup>, corresponding to the concentration of Brønsted acid sites, decreased as the Si/Al ratio increased, which was consistent with the results of NH<sub>3</sub>-TPD. An obvious band at 1445 cm<sup>-1</sup> for HZ-25 and HZ-38 indicated that there were more Lewis acid sites on them. It is well known that the Lewis acid sites on zeolites often originate from extra-framework aluminum species [22,23]. From XRD, HZ-25 and HZ-38 with lower relative crystallinity indicated that more amorphous extra-framework aluminum species were existed, thus bringing numerous Lewis acid sites. The ratio of the concentrations of Brønsted to Lewis acid sites was calculated from the area of the bands at 1545 cm<sup>-1</sup> and 1445 cm<sup>-1</sup> using extinction coefficients given in literature [24]. These values are summarized in Table 2. The concentration of Brønsted acid sites was significantly higher than that of Lewis acid sites, especially for the samples with higher relative crystallinity.



**Fig. 3.** Difference FT-IR spectra of pyridine (a) and collidine (b) adsorption on the HZSM-5 zeolites.



**Fig. 4.** Conversion of styrene oxide with time on stream over the catalysts. Reaction conditions: T = 200 °C, P = 1 atm, catalyst loading = 0.5 g, flow-rate of N<sub>2</sub> = 120 ml/min, WHSV = 3.0 h<sup>-1</sup>.

Although most of the acid sites on ZSM-5 exist inside the micropores, some of them are also located on the external surface and easily accessed by reactants without spatial constraints, which usually results in some undesired bulky hydrocarbons or coke being generated [25]. In this work, FT-IR with collidine adsorption [26,27] was used to probe external acid sites on the HZSM-5 samples. As illustrated in Fig. 3(b), the band at 1638 cm<sup>-1</sup> referred to collidine adsorbed on external Brønsted acid sites [28]. The amount of external Brønsted acid sites was calculated by the band's integrated absorbance (IA). As shown in Table 2, the external Brønsted acid sites on HZ-25, HZ-38 and HZ-50 were significantly more in number than those on HZ-135, HZ-150 and HZ-360 and decreased in the order HZ-25 > HZ-38 > HZ-50.

### 3.2. Isomerization of styrene oxide

Fig. 4 shows the conversion of styrene oxide with time on stream over each catalyst. Styrene oxide is a highly reactive substance and can be completely converted to phenylacetaldehyde and a list of other by-products over relatively weak acid sites at 70 °C and WHSV = 0.5–15 h<sup>-1</sup> [2,29]. From NH<sub>3</sub>-TPD/titration, NaZ-25 had only some weak acid sites (248 °C, 0.072 mmol/g) which could catalyze the isomerization of styrene oxide with initial conversion (TOS = 1.0 h) up to 96%. However, the conversion on NaZ-25 quickly decreased to 89%

within 3 h on stream. All the HZSM-5 zeolites ( $\text{SiO}_2/\text{Al}_2\text{O}_3 = 25\text{--}360$ ), containing both weak and strong acid sites, could almost completely catalyze this reaction with initial conversion (TOS = 1.0 h) of over 99% and maintained much longer time before deactivation relative to NaZ-25. So it can be concluded that the isomerization of styrene oxide is mainly catalyzed by the strong acid sites of HZSM-5 zeolites.

To obtain a quantitative description of catalytic stability, catalyst lifetime was defined as the time at which the initial conversion dropped by 2% and denoted by the dashed line in Fig. 4. The catalyst lifetimes of HZSM-5 first decreased and then increased with increasing Si/Al ratio, e.g., the lifetimes of low Si/Al HZSM-5 decreased in the order HZ-25 (12.5 h) > HZ-38 (11.0 h) > HZ-50 (5.8 h), whereas the lifetimes of high Si/Al HZSM-5 increased in the order HZ-135 (7.2 h) < HZ-150 (9.1 h) < HZ-360 (15.7 h). It has been reported that stronger acid sites favor the formation of condensation products which are responsible for the fast deactivation of catalyst [13–15], thus the catalyst with the strongest acid sites would exhibit the fastest deactivation. As determined by  $\text{NH}_3\text{-TPD}$ , the strong acid strength on HZSM-5 zeolites monotonically decreased with the increase of Si/Al ratio, so their catalyst lifetimes should monotonically increase according to the above literatures. However, the catalyst lifetimes of HZSM-5 zeolites presented here first decreased and then increased with increasing of Si/Al ratio. Furthermore, the similar BET surface area, micropore volume and size of HZSM-5 zeolites did not cause different catalytic performances. Therefore, it is assumed that the catalyst lifetimes are affected by both acid strength and concentration. With catalysts of similar acid strength, conversion of styrene oxide begins to drop until the number of acid sites deactivates to some extent. For example, the strong acid concentrations of HZ-25, HZ-38 and HZ-50 decreased from 0.606 to 0.416 and 0.336 mmol/g, but their acid strengths showed slight changes (from 438 to 417 °C), thus their lifetimes were mainly influenced by the acid concentration and decreased with increasing Si/Al ratio. HZ-135, HZ-150 and HZ-360 have much weaker acid sites (from 397 to 342 °C) and the acid strength was a more significant contributor in this case, which caused the catalyst lifetimes being prolonged with increasing Si/Al ratio even though their acid concentrations gradually decreased. Therefore, increasing the acid concentration while decreasing the acid strength can improve the catalyst lifetimes for this reaction.

The main by-products in this reaction were dimer (2,4-diphenyl-2-butenal) and trimer (2,4,6-tribenzyl-s-trioxane, mp 155–156 °C) of phenylacetaldehyde. The dimer was formed through aldol condensation of phenylacetaldehyde, while the trimer was obtained from trimerization of phenylacetaldehyde by an acid-catalyzed process [30]. Some other by-products, such as phenylethanol, phenylethandiol, styrene and so on, were also identified by GC-MS with total selectivity of less than 1%.

Fig. 5 shows the main product distribution with time on stream over the HZSM-5 samples. The initial selectivities of phenylacetaldehyde (TOS = 1.0 h) over HZ-25, HZ-38 and HZ-50 were only 56%, 76% and 92% respectively, which are caused by the formation of the trimer. However, the trimer selectivities over HZ-25, HZ-38 and HZ-50 gradually decreased from 42%, 22% and 6% to zero after 11, 9 and 4 h on stream, and correspondingly the phenylacetaldehyde selectivities increased up to 96%. HZ-135, HZ-150 and HZ-360 had no trimer production and the phenylacetaldehyde selectivities were all over 96% from beginning to end of the reaction. As determined by FT-IR collidine adsorption, the external acid sites on HZ-25, HZ-38 and HZ-50 were significantly more in number than those on HZ-135, HZ-150 and HZ-360 and decreased in the order HZ-25 > HZ-38 > HZ-50. Combining the above reaction results with those of the FT-IR collidine adsorption, it is evident that the trimerization of phenylacetaldehyde probably occurs at the external acid sites which are readily accessed without spatial constraints. For the trimer formation, three adsorbed precursor species should be in adjacent acid sites on the external surface. While the external acid sites are preferentially deactivated than the acid sites in pores [25], thus the trimer decreases with the reaction goes on and only occurs at the early

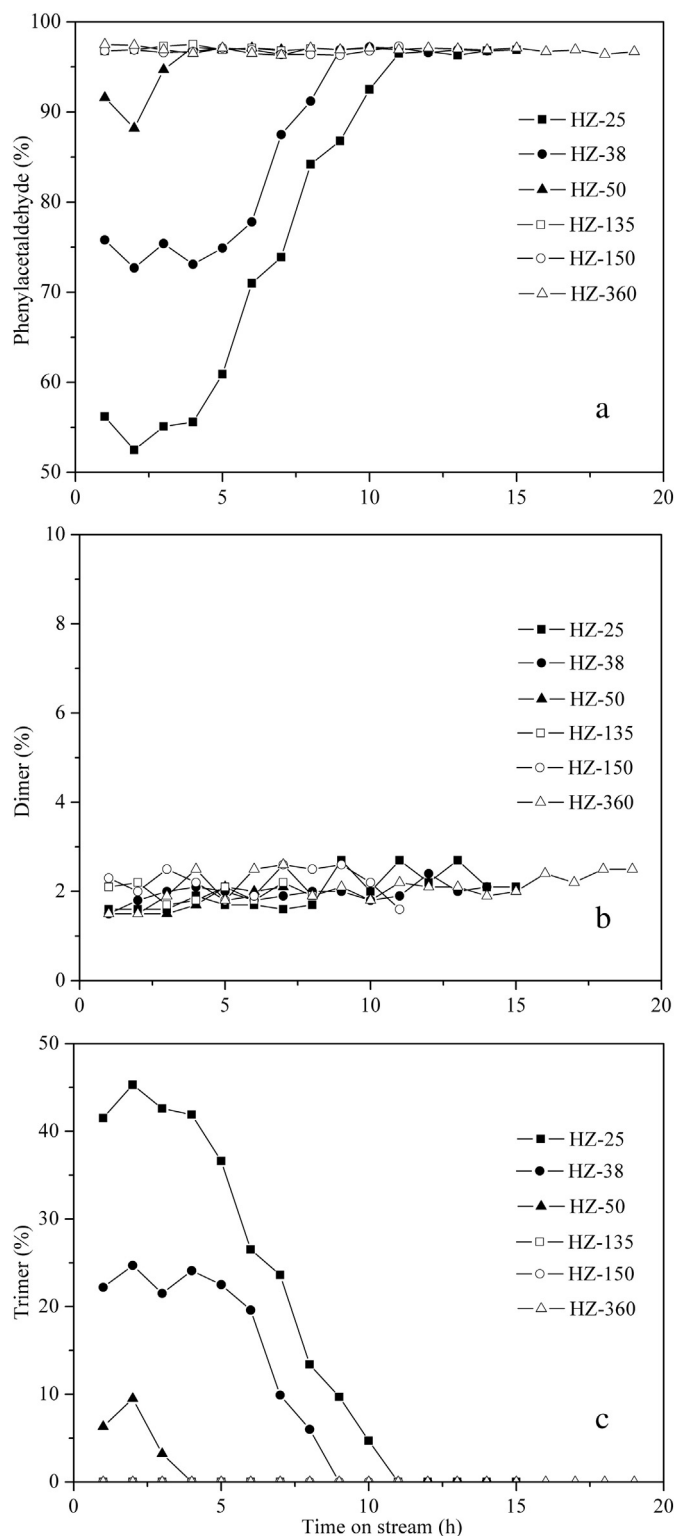


Fig. 5. Main product distribution with time on stream over the HZSM-5 zeolites. Reaction conditions:  $T = 200$  °C,  $P = 1$  atm, catalyst loading = 0.5 g, flow-rate of  $\text{N}_2 = 120$  ml/min,  $\text{WHSV} = 3.0$   $\text{h}^{-1}$ .

stage of the reaction on HZ-25, HZ-38 and HZ-50. However, the trimerization could not occur on HZ-135, HZ-150 and HZ-360, since they contained only a trace amount of external acid sites.

As shown in Fig. 5(b), the dimer selectivities were maintained at the same level (1–3%) from beginning to end of the reaction on all the samples. Therefore, the aldol condensation of phenylacetaldehyde is

not sensitive to varying acidity of catalysts and may be a spontaneous process controlled by thermodynamics.

#### 4. Conclusion

HZSM-5 is an efficient catalyst for isomerization of styrene oxide to phenylacetaldehyde. The isomerization is mainly catalyzed by the strong acid sites and catalyst lifetimes are affected by both acid strength and concentration. Aldol condensation and trimerization of phenylacetaldehyde are the main side reactions. The trimerization reaction occurs at external acid sites, while the aldol condensation reaction is not sensitive to varying acidity of catalysts. High Si/Al HZSM-5 (e.g.,  $\text{SiO}_2/\text{Al}_2\text{O}_3 = 360$ ), which contains weaker acid sites inside pores and trace amount of external acid sites, is more suitable for this reaction with a higher stability and phenylacetaldehyde yield up to 95%.

#### Appendix A. Supplementary data

Supplementary data associated with this article can be found in the online version, at <http://dx.doi.org/10.1016/j.catcom.2014.07.024>. These data include MOL files and InChIKeys of the most important compounds described in this article.

#### References

- [1] W.F. Hölderich, U. Barsnick, in: R.A. Sheldon, H. van Bekkum (Eds.), *Fine Chemicals Through Heterogeneous Catalysis*, first ed., Wiley-VCH, Weinheim, 2001, pp. 217–231.
- [2] H. Smuda, W. Hoelderich, N. Goetz, H.G. Recker, US Patent 4929765, 1990.
- [3] W. Hoelderich, N. Goetz, L. Hupfer, R. Kropp, H. Theobald, B. Wolf, US Patent 5225602, 1993.
- [4] J.M. Watson, US Patent 3927110, 1975.
- [5] H. Kochkar, J.M. Clacens, F. Figueras, *Catal. Lett.* 78 (2002) 91–94.
- [6] B.G. Pope, US Patent 4650908, 1987.
- [7] F. Zaccheria, R. Psaro, N. Ravasio, L. Sordelli, F. Santoro, *Catal. Lett.* 141 (2011) 587–591.
- [8] E. Ruiz-Hitzky, B. Casal, *J. Catal.* 92 (1985) 291–295.
- [9] G.K.S. Prakash, T. Mathew, S. Krishnaraj, E.R. Martinez, G.A. Olah, *Appl. Catal. A* 181 (1999) 283–288.
- [10] K. Smith, G.A. El-Hiti, M. Al-Shamali, *Catal. Lett.* 109 (2006) 77–82.
- [11] M. Chamoumi, D. Brunel, P. Geneste, P. Moreau, J. Soloflo, *Stud. Surf. Sci. Catal.* 59 (1991) 573–579.
- [12] D. Brunel, M. Chamoumi, B. Chiche, A. Finiels, C. Gauthier, P. Geneste, P. Graffin, F. Marichez, P. Moreau, *Stud. Surf. Sci. Catal.* 52 (1989) 139–149.
- [13] V.V. Costa, K.A. da Silva Rocha, I.V. Kozhevnikov, E.V. Gusevskaya, *Appl. Catal. A* 383 (2010) 217–220.
- [14] I. Salla, O. Bergada, P. Salagre, Y. Cesteros, F. Medina, J.E. Sueiras, T. Montanari, *J. Catal.* 232 (2005) 239–245.
- [15] M.D. González, Y. Cesteros, P. Salagre, F. Medina, J.E. Sueiras, *Microporous Mesoporous Mater.* 118 (2009) 341–347.
- [16] N.Y. Topsøe, K. Pedersen, E.G. Derouane, *J. Catal.* 70 (1981) 41–52.
- [17] G. Seo, H.S. Jeong, S.B. Hong, Y.S. Uh, *Catal. Lett.* 36 (1996) 249–253.
- [18] N.R. Meshram, S.G. Hegde, S.B. Kulkarni, P. Ratnasamy, *Appl. Catal. A* 8 (1983) 359–367.
- [19] L. Tao, L. Chen, S.F. Yin, S.L. Luo, Y.Q. Ren, W.S. Li, X.P. Zhou, C.T. Au, *Appl. Catal. A* 367 (2009) 99–107.
- [20] P.L. Tan, Y.L. Leung, S.Y. Lai, C.T. Au, *Appl. Catal. A* 228 (2002) 115–125.
- [21] R.J. Kalbasi, M. Ghiaci, A.R. Massah, *Appl. Catal. A* 353 (2009) 1–8.
- [22] J.L. Motz, H. Heinichen, W.F. Hölderich, *J. Mol. Catal. A Chem.* 136 (1998) 175–184.
- [23] J. Van Bokhoven, M. Tromp, D. Koningsberger, J. Müller, J. Pieterse, J. Lercher, B. Williams, H. Kung, *J. Catal.* 202 (2001) 129–140.
- [24] C.A. Emeis, *J. Catal.* 141 (1993) 347–354.
- [25] W. Ding, G.D. Meitzner, E. Iglesia, *J. Catal.* 206 (2002) 14–22.
- [26] F. Thibault-Starzyk, I. Stan, S. Abelló, A. Bonilla, K. Thomas, C. Fernandez, J.-P. Gilson, J. Pérez-Ramírez, *J. Catal.* 264 (2009) 11–14.
- [27] S. Inagaki, K. Kamino, E. Kikuchi, M. Matsukata, *Appl. Catal. A* 318 (2007) 22–27.
- [28] M.S. Holm, S. Svelle, F. Joensen, P. Beato, C.H. Christensen, S. Bordiga, M. Bjørgen, *Appl. Catal. A* 356 (2009) 23–30.
- [29] C. Neri, F. Buonomo, US Patent 4495371, 1985.
- [30] J.L.E. Brickson, G.N. Grammer, *J. Am. Chem. Soc.* 80 (1958) 5466–5469.